BB

Michigan State University

National Superconducting Cyclotron Laboratory

PROBING TOROIDAL DENSITY DISTRIBUTIONS WITH TWO-PROTON CORRELATION FUNCTIONS?

D.O. HANDZY, S.J. GAFF, W. BAUER, F.C. DAFFIN, C.K. GELBKE, and G.J. KUNDE

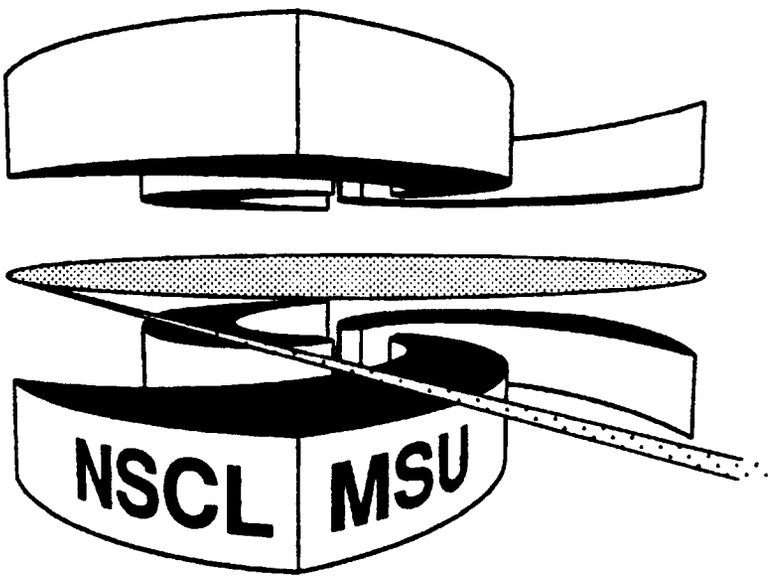

MSUCL-960 **NOVEMBER 1994**

Probing Toroidal Density Distributions with Two-Proton Correlation Functions ?

D.O. Handzy, S.J. Gaff, W. Bauer, F.C. Daffin, C.K. Gelbke, and G.J. Kunde

National Superconducting Cyclotron Laboratory and Department of Physics and Astronomy, Michigan State University, East Lansing, MI 48824, USA

Abstract

Transport calculations based on the Boltzmann-Uehling-Uhlenbeck (BUU) equation predict the formation of toroidal density distributions for central ^{36}Ar + ^{45}Sc collisions at E/A = 80 MeV. Calculations with the Koonin-Pratt formalism are performed to explore whether the occurrence of such non-spherical breakup configurations could be tested via two-proton correlation measurements. The predicted signal appears detectable, but weak, because most protons emerge early in the reaction when the source is more compact. Contributions from non-zero impact parameters give rise to additional complications.

PACS number: 25.70.Pq

Model calculations based on the Boltzmann-Uehling-Uhlenbeck (BUU) transport equation predict that disk-shaped [1] or toroidal configurations may be produced in central heavy ion collisions [2-6]. A number of observables have been suggested [1,2,5,7,8] which might signal a toroidal breakup configuration, but experimental evidence for the formation of tori has not yet been found. Suggestions of observables were based upon either intuitive arguments [1,2,5] or schematic calculations [7,8] in which a multifragment disintegration of the toroidal density distribution was assumed. In no case were these suggestions substantiated by dynamical calculations capable of exploring the space-time evolution of the reaction zone and of the emitted radiation. A consistent dynamical treatment is possible for nucleon emission and for the calculation of two-proton correlation functions, using the Koonin-Pratt formalism [9-13] and the actual phase-space distributions predicted by the BUU theory. In this note we investigate to what degree two-proton correlation functions can be expected to provide information about the formation of toroidal density distributions.

Two-proton correlation functions probe the space-time extent of the emitting source through the spatial dependence of final-state interactions and antisymmetrization effects [9-13]. At short distances, the attractive singlet S-wave interaction dominates; it gives rise to a maximum at relative momentum $q \approx 20$ MeV/c. Antisymmetrization and Coulomb repulsion between the two protons produce a minimum at $q \approx 0$ MeV/c [9]. Sensitivity to the shape of the phase space distribution of emitted particles is mostly due to antisymmetrization which leads to a stronger suppression of the correlation function when the relative momentum vector, $\mathbf{q} = \frac{1}{2}(\mathbf{p}_1 - \mathbf{p}_2)$, is oriented parallel to the shortest dimension of a non-spherical phase-space distribution [9,10,13-16].

For our study we analyze the results of BUU calculations which were performed with high statistics for small-impact-parameter ^{36}Ar + ^{45}Sc collisions at E/A = 80 MeV. Measured impact-parameter filtered correlation functions [6,16,17] for this reaction were successfully reproduced by BUU calculations [6,17] which predicted the occurrence of toroidal density distributions. The data were, however, also reproduced by assuming emission from a spherical source of finite lifetime [16]. Thus agreement with BUU calculations could not be taken as evidence for the predicted toroidal shapes [6].

Depicted in Fig. 1 is the calculated evolution of the *residual* system for strictly central ^{36}Ar + ^{45}Sc collisions at E/A=80 MeV. Panels from left to right show density projections at times t = 10, 50, 100 and 150 fm/c; top and bottom panels show projections onto the (x,y) and (x,z) planes respectively, with the z-axis chosen parallel to

the beam axis. The system is seen to evolve into a toroidal configuration which is symmetric about the beam axis. In order to isolate effects due to the spatial configuration of the emitting source, we make cuts on the directions of total and relative momenta, shown in Fig. 2.

The total momentum **P** is selected to lie within ±10° of the (x,y) plane and the relative momentum **q** is selected (within ±10°) along three directions: q_{par} is parallel to **P** and thus sensitive to the source dimension and its lifetime; q_{perp} and q_{beam} are perpendicular to **P** and thus insensitive to lifetime effects. q_{perp} lies in the (x,y) plane and is sensitive to the radius of the torus, while q_{beam} is parallel to the beam axis and is thus sensitive to the thickness of the torus.

The solid and dashed curves in Fig. 3 show two-proton correlation functions calculated under the simplifying assumption of instantaneous emission from the volume of the toroidal spatial density distribution at t=100 fm/c (see insert and Fig. 1). The momenta for this simulation were chosen isotropic in the center of mass frame, with a flat distribution for each cartesian component ranging from -200 to 200 MeV/c. Statistical uncertainties of the calculations are indicated by errors bars. The correlation functions for q_{perp} and q_{par} are practically degenerate (not shown in the figure). The correlation function for q_{beam} exhibits a strongly enhanced Pauli suppression reflecting the shorter dimension of the torus. The open and solid points in the figure represent the result of calculations for instantaneous emission from a disc-shaped distribution obtained by uniformly filling the "hole" of the doughnut. (The two density distributions are compared in the insert.) The calculations for the two source geometries are very similar indicating that our choice of directional cuts is not sensitive to the "hole" of the torus. It will be even more difficult, if not impossible, to differentiate between a disk and a torus with experimental correlation functions which average over the temporal evolution of the reaction zone and over a finite window of impact parameters. However, one may hope to distinguish these "flat" shapes from spherically symmetric sources, even in a realistic reaction scenario.

Figure 4 illustrates that the degeneracy of $R(q_{perp})$ and $R(q_{par})$ is removed if emission occurs with a finite life time. Specifically, we used the same toroidal spatial distribution employed previously, with an added exponential time dependence, $dN/dt \propto \exp(-t/\tau)$, with $\tau = 25$ fm/c [16]. The magnitude of the peak at $q \approx 20$ MeV/c is reduced, and the correlation functions are ordered approximately as $R(q_{par}) \geq R(q_{perp}) \geq R(q_{beam})$ reflecting increasing Pauli-suppression due to smaller average particle separations along the respective directions.

Figures 3 and 4 suggest that two-particle correlation functions are well suited to obtain useful information about non-spherical sources of fixed geometrical shape. This simplified scenario serves only as an example. More realistic calculations which incorporate the dynamics of proton emission for strictly central collisions as predicted by the BUU transport model are shown in Fig. 5. Here, the same directional cuts on relative momenta were employed as defined in Fig. 2 with no restrictions on total momentum, P. The predicted differences between the three directional cuts are significantly reduced because protons are emitted on a relatively fast time scale (see insert of Fig. 5) and thus predominantly from the more compact initial configurations.

Further complications arise when unavoidable contributions of non-zero impact parameters are taken into account. Figure 6 illustrates the strong impact-parameter dependence of shape and orientation of the residual systems calculated from the BUU transport theory at t = 100 fm/c. Toroidal shapes are predicted for small (but non-zero) impact parameters, but their symmetry axes are tilted away from the beam axis. For impact parameters larger than about 3 fm, the residual systems assume stretched configurations leading to "binary" exit channels, possibly accompanied by neck-emission [18].

Figure 7 illustrates the effect of impact parameter averaging. The correlation functions shown in the figure were calculated by using the fixed-axis directional cuts defined in Fig. 2 and by employing the central-cut impact-parameter distribution of ref. [6] (shown in the insert of Fig. 7). For tilted tori (i.e. for collisions with b>0), the directional cut parallel to the beam-axis no longer probes the smallest dimension of the residual system. As a consequence, the correlation function $R(q_{beam})$ is less suppressed, and the relative magnitudes of the three correlation functions are different than in Figs. 4 and 5. Further, dynamical correlations due to impact parameter averaging [19] become important due to the non-negligible sideward directed flow, causing additional distortions at larger relative momenta (q > 40 MeV/c). The qualitative features of impact parameter averaged correlation functions are thus different than those for purely central collisions, making the extraction of a signal of toroidal (or disk-shaped) density distributions difficult, if not impossible. Nevertheless, BUU calculations predict correlation functions with shapes distinct from those representing emission from spherical sources of finite lifetime. Unfortunately, the statistical accuracy of the experimental data of refs. [6,16,17] is not sufficient to allow such tests. Impact-parameter selected correlation functions of improved statistical accuracy and with appropriately chosen directional cuts should, however, be able to test the non-trivial

space-time evolution predicted by microscopic transport calculations. We believe, however, that such an experimental signature would be very difficult to interpret in a model independent way.

Valuable discussions with Dr. S. Pratt are gratefully acknowledged. This work was supported by the National Science Foundation under Grants No. PHY-9403666 and PHY-9214992. W.B. acknowledges support from an NSF Presidential Faculty Fellow Award, and G.J.K. acknowledges support from the Alexander von Humboldt Foundation.

References

1. L.G. Moretto, K. Tso, N. Colonna, and G.J. Wozniak, Phys. Rev. Lett. **69**, 1884 (1992).
2. W. Bauer, G.F. Bertsch and H. Schulz, Phys. Rev. Lett. **69** (1992) 1888.
3. D.H.E. Gross, B.A. Li and A.R. DeAngelis, Ann. Physik **1** (1992) 467.
4. B. Borderie, B. Remaud, M.F. Rivet and F. Sebille, Phys. Lett. B **302** (1985) 53.
5. H.M. Xu, J.B. Natowitz, C.A. Gagliardi, R.E. Tribble, C.Y. Wong, and W.G. Lynch, Phys. Rev. **C48**, 933 (1993).
6. D.O. Handzy, M.A. Lisa, C.K. Gelbke, W. Bauer, F.C. Daffin, P. Decowski, W.G. Gong, E. Gualtieri, S. Hannuschke, R. Lacey, T. Li, W.G. Lynch, C.M. Mader, G.F. Peaslee, T. Reposeur, S. Pratt, A.M. Vander Molen, G.D. Westfall, J.Yee, and S.J. Yennello, Phys. Rev. **C50** (1994) 858.
7. L. Phair, W. Bauer, and C.K. Gelbke, Phys. Lett. **B314** (1993) 271.
8. T. Glasmacher, C.K. Gelbke and S. Pratt, Phys. Lett. B **314** (1993) 265.
9. S.E. Koonin, Phys. Lett. **70B**, 43 (1977).
10. W.G. Gong, W. Bauer, C.K. Gelbke, and S. Pratt, Phys. Rev. **C43**, 781 (1991)
11. D.H. Boal, C.K. Gelbke, and B.K. Jennings, Rev. Mod. Phys. **62**, 553 (1990) and references therein.
12. W. Bauer, C.K. Gelbke, and S. Pratt, Ann. Rev. Nucl. Part. Sci. **42**, 77 (1992) and references therein..
13. S. Pratt and M.B. Tsang, Phys. Rev. **C36**, 2390 (1987).
14. S. Pratt, Phys. Rev. Lett. **53**, 1219 (1984).
15. G.F. Bertsch, Nucl. Phys. **A489**, 173c (1989).
16. M.A. Lisa, C.K. Gelbke, W. Bauer, P. Decowski, W.G. Gong, E. Gualtieri, S. Hannuschke, R. Lacey, T. Li, W. G. Lynch, C.M. Mader, G.F. Peaslee, S. Pratt, T. Reposeur, A.M. Vander Molen, G.D. Westfall, J. Yee, and S.J. Yennello, Phys. Rev. Lett. **71**, 2863 (1993).
17. M.A. Lisa, C.K. Gelbke, W. Bauer, P. Decowski, W.G. Gong, E. Gualtieri, S. Hannuschke, R. Lacey, T. Li, W.G. Lynch, C.M. Mader, G.F. Peaslee, T. Reposeur, A.M. Vander Molen, G.D. Westfall, J. Yee, and S.J. Yennello, Phys. Rev. Lett. **70**, 3709 (1993).
18. C.P. Montoya, W.G. Lynch, D.R. Bowman, G.F. Peaslee, N. Carlin, R.T. de Souza, C.K. Gelbke, W.G. Gong, Y.D. Kim, M.A. Lisa, L. Phair, M.B. Tsang, J. Webster, C. Williams, N. Colonna, K. Hanold, M.A. McMahan, G.J. Wozniak, and L.G. Moretto, Phys. Rev. Lett. **73**, (1994) in press.

19. W.G. Gong, C.K. Gelbke, W. Bauer, N. Carlin, R.T. de Souza, Y.D. Kim, W.G. Lynch, T. Murakami, G. Poggi, D.P. Sanderson, M.B. Tsang, H.M. Xu, D.E. Fields, K. Kwiatkowski, R. Planeta, V.E. Viola, Jr., S.J. Yennello, and S. Pratt, Phys. Rev. **C43**, 1804 (1991).

Figure Captions

Fig. 1: Residual system predicted by BUU transport calculations for central ^{36}Ar + ^{45}Sc collisions at E/A = 80 MeV at times t=10, 50, 100, and 150 fm/c. The top panels show distributions viewed along the beam axis; the bottom panels show distributions projected onto a plane which contains the beam axis.

Fig. 2: Geometry of toroid and directions of applied cuts on q used in all of our calculations.

Fig. 3: Comparison of correlation functions calculated for a zero-lifetime torus and a disc. The assumed density distributions are depicted in the insert; torus on the left and disc on the right.

Fig. 4: Two-proton correlation functions predicted for emission from a torus assuming an exponential time dependence of mean emission time τ = 25 fm/c.

Fig. 5: Two-proton correlation functions predicted by BUU transport calculations for b=0 ^{36}Ar + ^{45}Sc collisions at E/A = 80 MeV. The insert shows the time-dependence of proton emission.

Fig. 6: Residual systems predicted at t = 100 fm/c by BUU transport calculations for ^{36}Ar + ^{45}Sc collisions at E/A = 80 MeV for the indicated impact parameters.

Fig. 7: Two-proton correlation functions predicted by BUU transport calculations for central ^{36}Ar + ^{45}Sc collisions at E/A = 80 MeV. The assumed distribution of impact parameters [6] is shown in the insert.

Fig 1

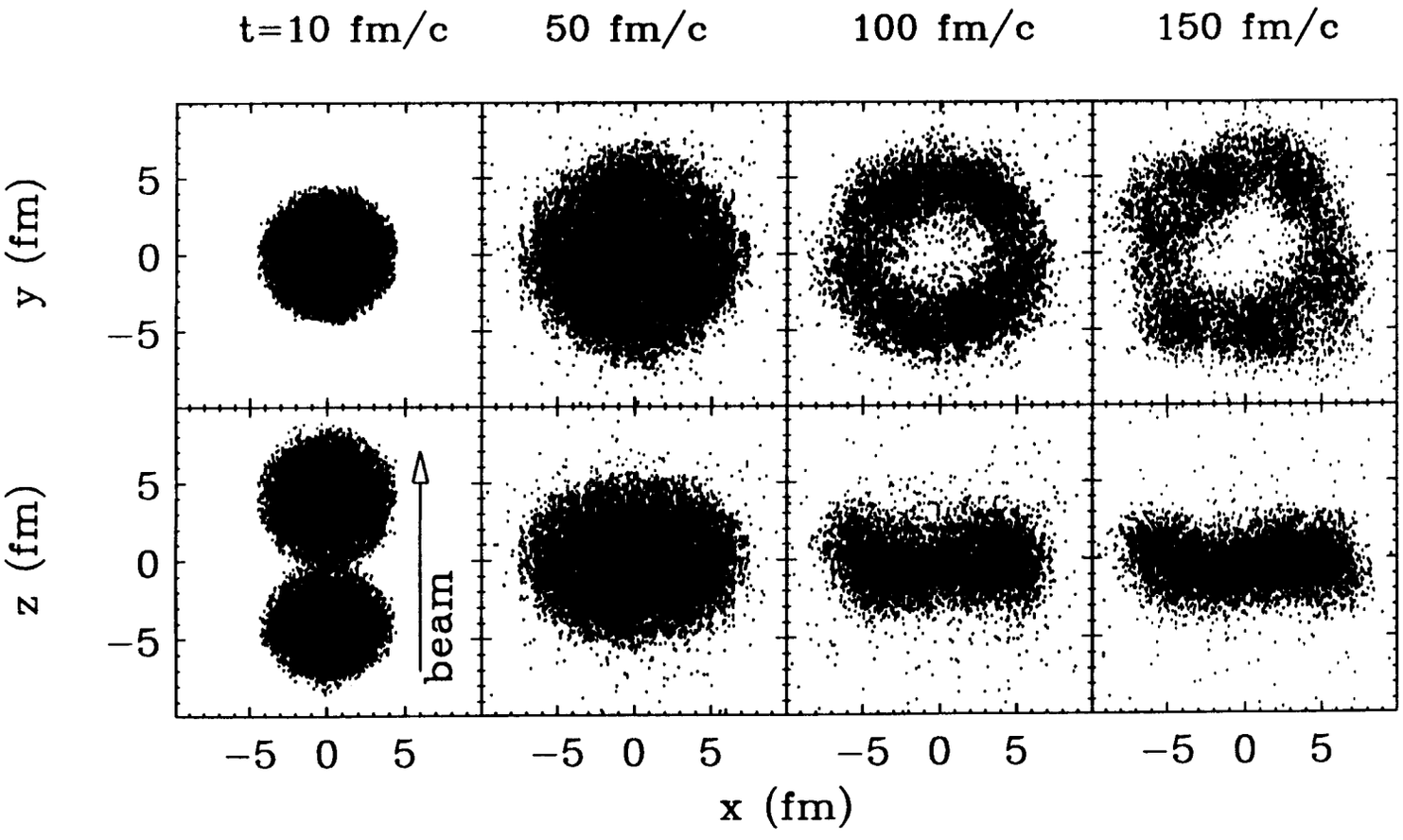

Fig 2

Tori Coordinate Definitions

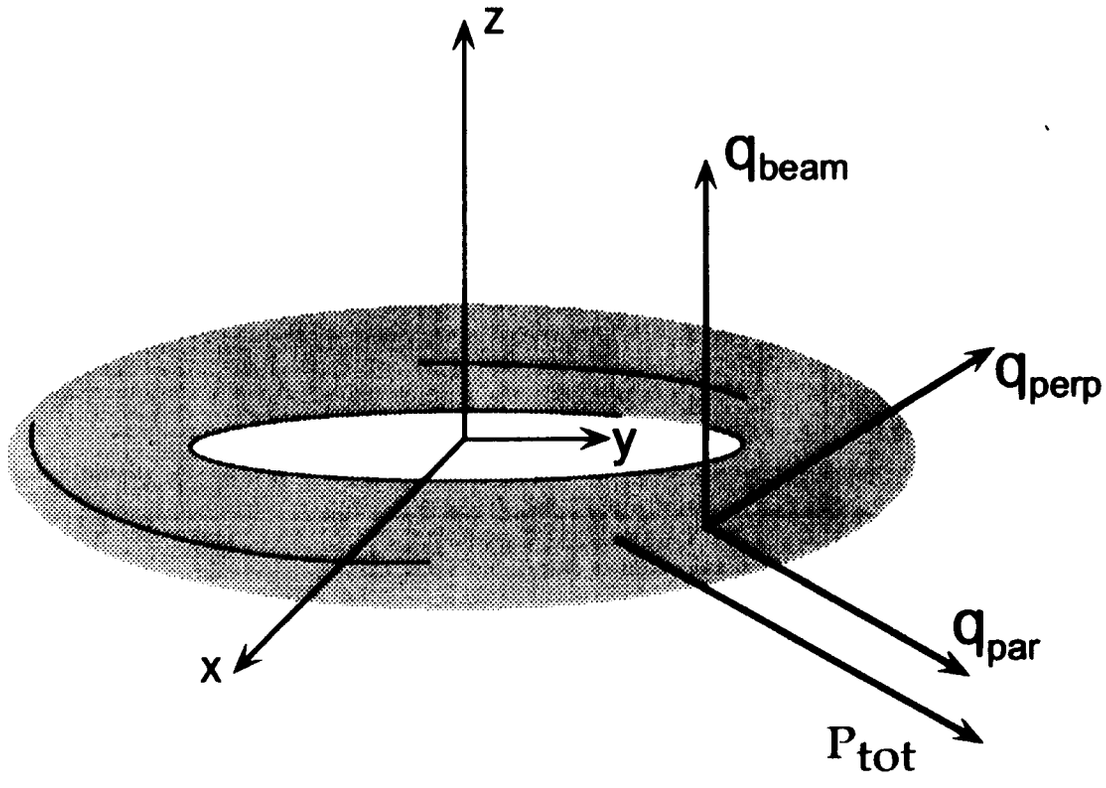

Fig 3

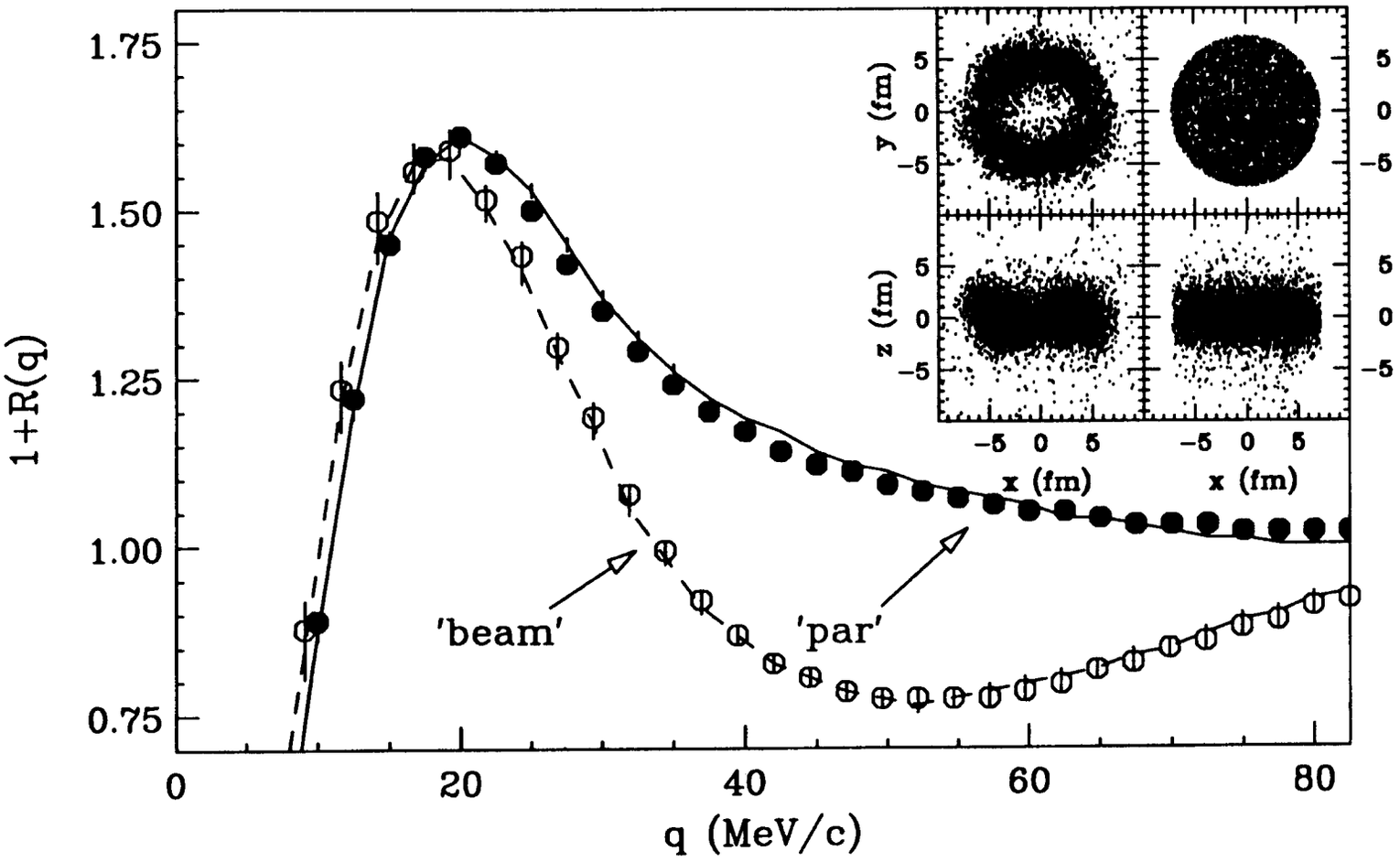
1.75
1.50
1.25
1.00
0.75
1+R(q)
0
20
40
60
80
q (MeV/c)
'beam'
'par'
y (fm)
z (fm)
x (fm)
x (fm)
5
0
−5

Fig 4

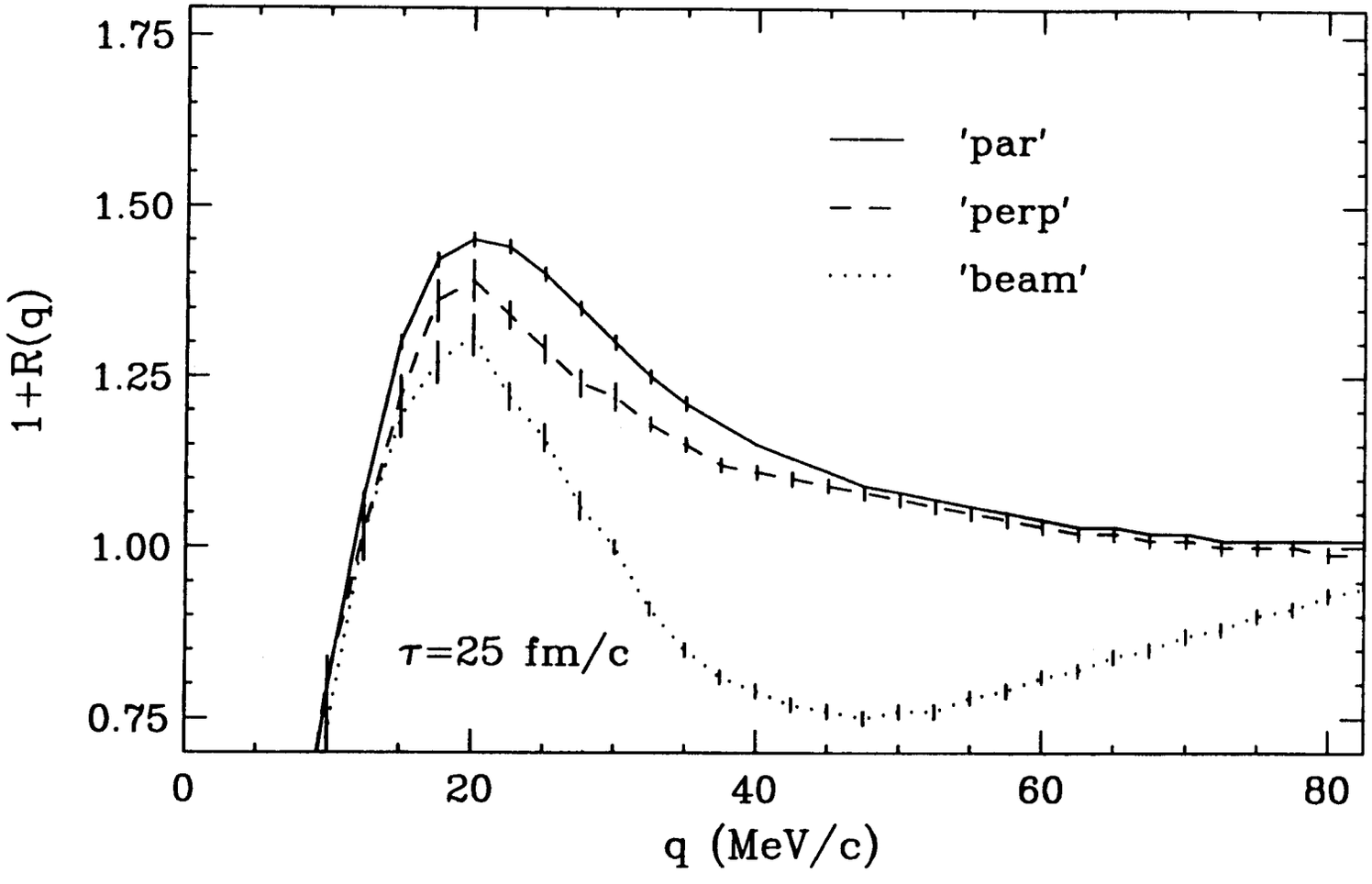

Fig 5

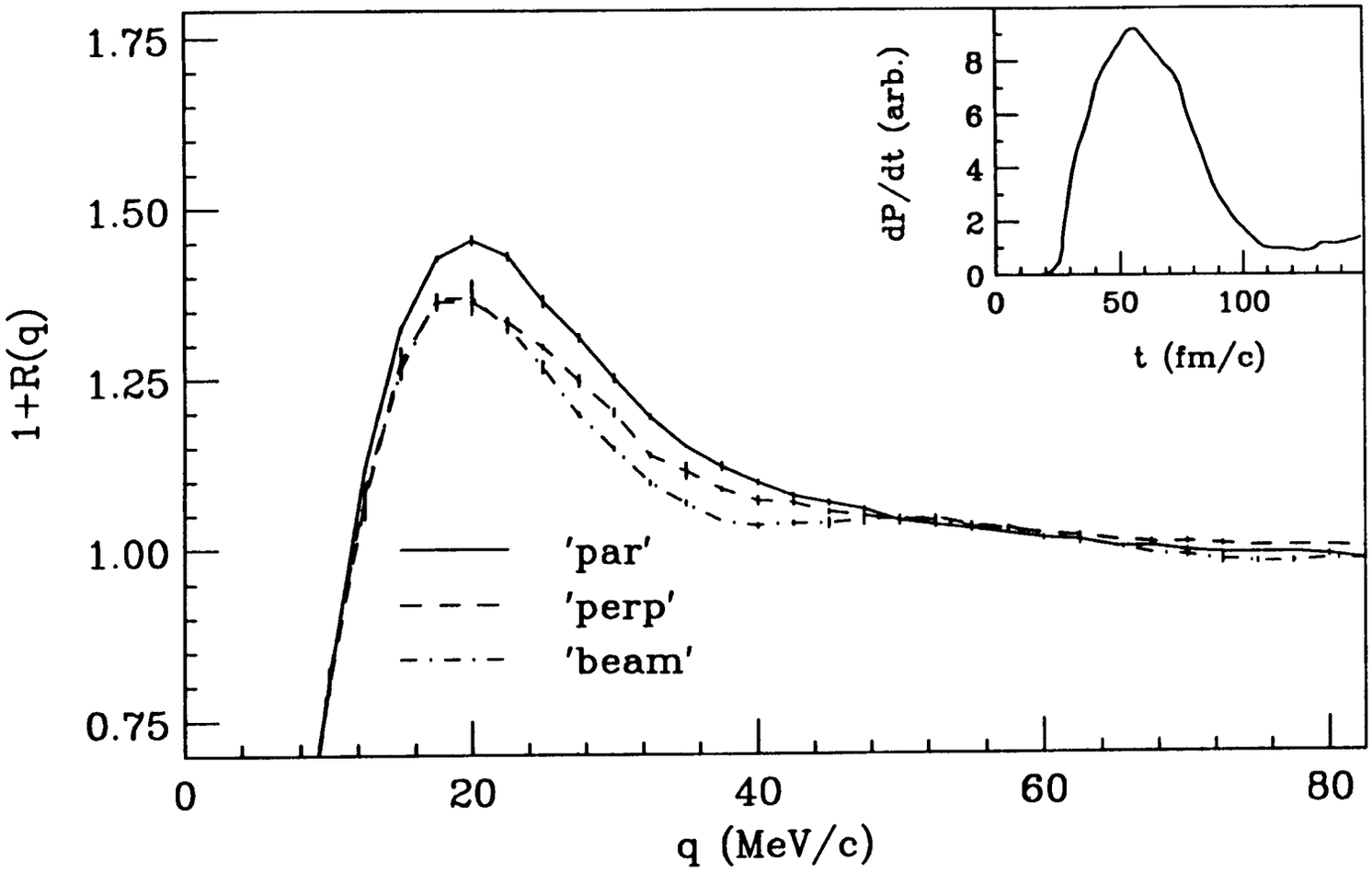
1.75
1.50
1.25
1.00
0.75
1+R(q)
0
20
40
60
80
q (MeV/c)
'par'
'perp'
'beam'
dP/dt (arb.)
8
6
4
2
0
0
50
100
t (fm/c)

Fig 6

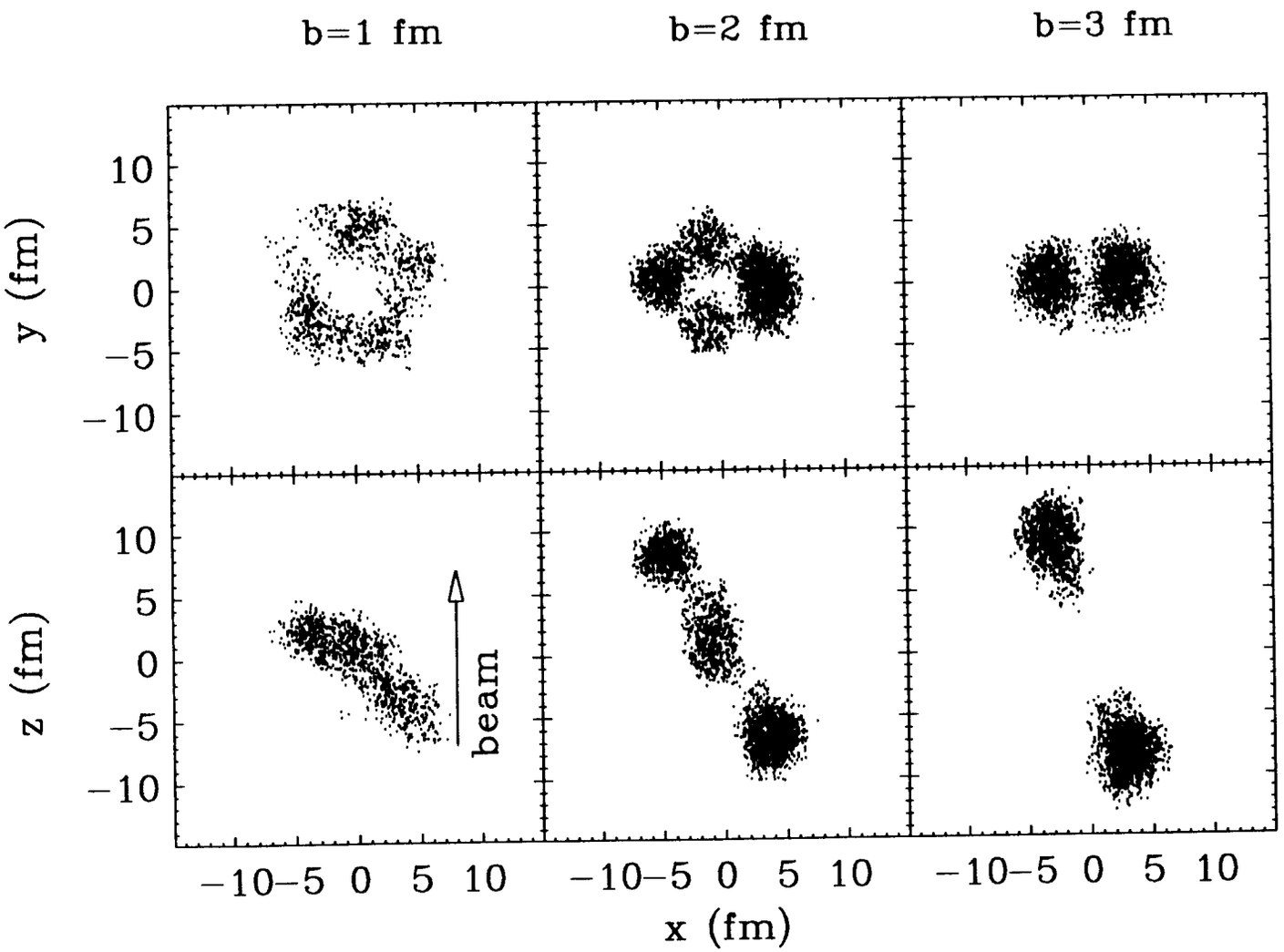

Fig 7

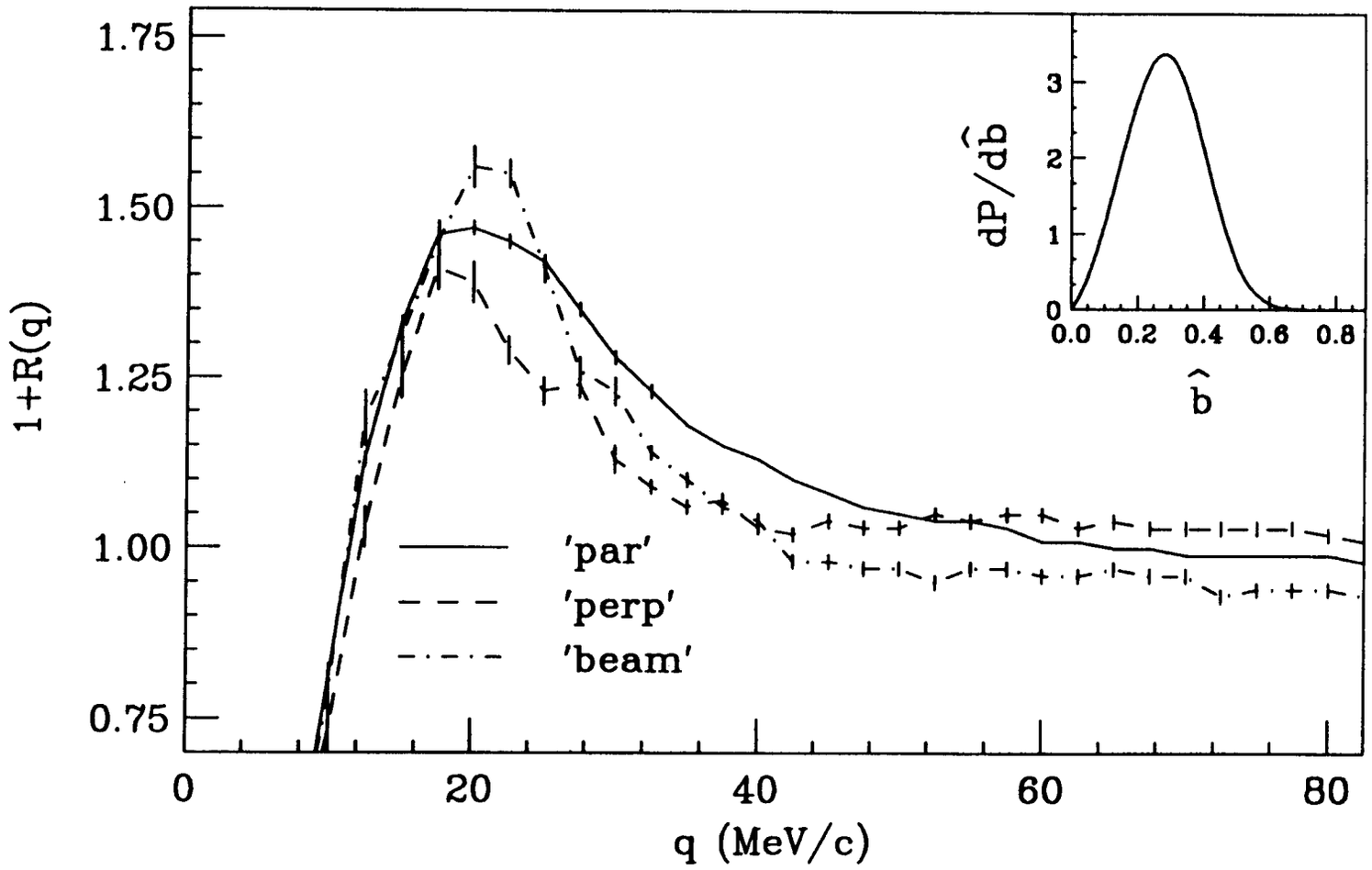
1.75
1.50
1.25
1.00
0.75
1+R(q)
0
20
40
60
80
q (MeV/c)
'par'
'perp'
'beam'
dP/db̂
3
2
1
0
0.0
0.2
0.4
0.6
0.8
b̂